A Miniaturized Ultrasonically Powered Programmable Optogenetic Implant Stimulator System

Marcus J. Weber, Anirudha Bhat, Ting Chia Chang, Jayant Charthad, and Amin Arbabian

Department of Electrical Engineering, Stanford University, Stanford, CA, 94301, USA

***Abstract* — A fully programmable, wirelessly powered optogenetic stimulator system is demonstrated. Implantable devices, with integrated optical stimulators, are powered and controlled using a programmable external ultrasonic transmitter. A methodical analysis is performed to investigate obtainable optical available powers using a highly efficient ultrasonic link. Optical intensities and stimulation patterns practical for optogenetic applications are easily achieved with safe levels of ultrasound. To our knowledge, this is the first ultrasonically powered optogenetic stimulator. The active area of the implantable device measures just 15 mm^2.**

***Index Terms* — Electroceuticals, optogenetics, implantable medical devices, peripheral nerve stimulation, medical implants, ultrasound, wireless power.**

I. Introduction

In the future, closed-loop neuromodulation treatments, or "electroceuticals", which offer more targeted and adaptable therapy, may replace drugs as the dominant treatment for neurological and other forms of disease [1]. Electrical peripheral nerve stimulation (PNS) has shown promise in commercial and research pursuits for treating many neurological diseases such as: epilepsy, chronic pain, and bladder incontinence [1]. Though, typical electrical stimulation has low spatial resolution and has limited effectiveness in blocking action potentials [1], [2]. Optogenetics is a new method of neuromodulation, which offers significant advantages over electrical stimulation in spatial resolution and signal blocking [1]-[3]. Activation and inhibition of action potentials in the peripheral nervous system of rats has already been demonstrated using conventional fiber-based optogenetic systems [2], [3]. However, these systems are too large, fragile, and invasive to be practical for future human PNS.

In this paper, we demonstrate a proof-of-concept, fully wireless implant system with optogenetic stimulation capabilities. Powered using a highly efficient ultrasonic power-up link, we omit bulky batteries to shrink the implant size to mm-dimensions, while still providing the high ~mW power levels needed for optogenetic stimulation. Ultrasonic power delivery offers many advantages over RF and inductive links making it optimal for delivering power up to larger depths (> 5 cm) and smaller volumes [4], [5]. The implant's stimulation pattern is also externally programmed via the ultrasound transmitter to enable stimulation with variable pulse widths and frequencies. The entire implantable device occupies an active area of just 15 mm^2.

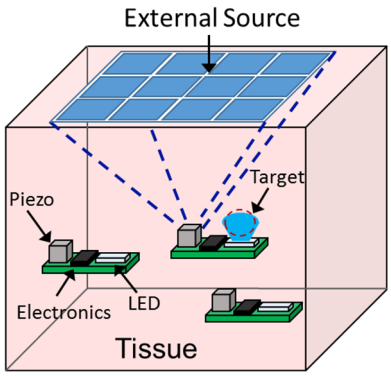

Fig. 1. Futuristic conceptual representation of a multi-node ultrasonically powered optogenetic system with beam-forming capability. The figure is not to scale.

II. System Design and Topology

Fig. 1 shows a futuristic conceptual diagram (not to scale) of our proposed wireless optogenetic system. Single or multiple implants could be injected or implanted into a subject to perform optical stimulation of different illumination targets. An external ultrasonic array could be used to beam-form to specific implants to increase the power-up link efficiency, and to selectively activate certain implants in a multi-node system. The implant consists of an ultrasonic receiver, electronics for power and data processing, and an LED, or multiple LEDs, for optical stimulation. The electronics on the implant can be implemented to perform many different functions using an integrated circuit (IC), as we have done in the past [4], [5].

In the current setup, we do not use beam-forming, but instead use a single-element transmitter for a proof-of-concept demonstration of ultrasonic power and programmability for optogenetic implants. In this paper, we focus on designing a general-purpose device where a customized IC is not necessary. The implant operates without data processing circuitry or significant energy storage; rather, we implement the programmability entirely on the transmitter side, and control the implant using pulsed transmission waveforms. With this methodology, the implant will receive power and illuminate the LED only while ultrasound is incident, allowing for programmability. Depending on the application, a custom IC could be built with memory and programmable capabilities, at the cost of increased complexity, size, and power requirements. Using

this system, we provide an end-to-end analysis of the required wireless power levels needed to enable optogenetic stimulation. We will show that this system can achieve practical optogenetic stimulation patterns with a comfortable safety margin.

III. Electrical Characterization

Fig. 2 (a) shows the schematic of the implant used in this demonstration. We operate a piezoelectric receiver (piezo) at the short-circuit resonance frequency for simplified and high-efficiency impedance matching - the Thevenin equivalent circuit model is shown in Fig. 2 (a) [4], [5]. The peak open-circuit voltage (V_{oc}) is determined by the electrical available power at the piezo ($P_{av,elec}$) and the resistance of the piezo receiver (R_{piezo}) as

$$V_{oc} = \sqrt{8 \times P_{av,elec} \times R_{piezo}}. \quad (1)$$

The electrical available power is related to the product of the acoustic intensity (I_{acou}) and receiver area (A) by the piezo receiver power conversion efficiency (PCE)

$$P_{av,elec} = PCE \times I_{acou} \times A. \quad (2)$$

For the piezo receiver used in this demonstration, the thickness is 1.44 mm with lateral dimensions of 1.02 mm × 1.02 mm. The resonance frequency was 955 KHz, R_{piezo} is 3.3 kΩ, and the PCE is 0.5 [5]. A bridge rectifier chip is used for rectification, and a 4.7 nF capacitor filters the signal for a DC output voltage. We chose a blue LED (~460 nm) as blue light is typically used for optogenetics [2], [3]. The LED is current-limited by R_{LED}, which is 100 Ω.

We characterized the electrical efficiency of our implant through simulation (LTspice) and measurement as a function of $P_{av,elec}$. The total efficiency is defined as the ratio of the power consumed by the LED (P_{LED}) and $P_{av,elec}$. The results are shown in Fig. 2 (b). Wireless power measurements were performed at 955 kHz with 6 cm distance between the transmitter and the implant. Mineral oil was used for the acoustic medium because it has similar acoustic impedance to soft tissues (~1.2 MRayl and ~1.5 MRayl, respectively) and the oil minimizes electrical parasitics of the medium [6]. In the body, soft tissues add small losses (~1 dB/cm at 1 MHz) [6], but beamforming can be used to compensate for these losses and position the maximum acoustic intensity focal spot on the implant for up to great depths in tissue [7].

As seen in Fig. 2 (b), the measured and simulated efficiencies show excellent agreement. We found the rectifier efficiency (P_{DC}/P_{in}) and the load efficiency (P_{LED}/P_{DC}) were mostly constant over all $P_{av,elec}$ with values of ~80% and ~95%, respectively. The decrease in the total efficiency at higher $P_{av,elec}$ is mostly due to a decrease in the fractional power input to the rectifier ($P_{in}/P_{av,elec}$), shown in Fig. 2 (b). This decrease is due to a degrading impedance match between the piezo impedance and the effective input resistance (R_{in}) of the rectifier circuit. High electrical efficiencies are necessary in order to lower the required acoustic intensity (I_{acou}) required to power the LED.

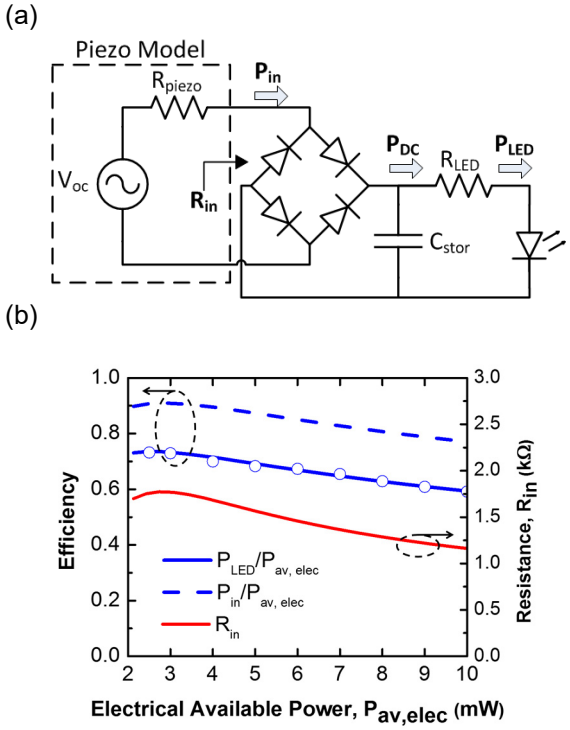

Fig. 2. (a) Schematic of the implant used in this demonstration. (b) Measured (circles) and simulated $P_{LED}/P_{av,elec}$, simulated $P_{in}/P_{av,elec}$, and simulated R_{in} as a function of $P_{av,elec}$.

IV. Optical Characterization

In order to verify our LED models through measurement, we built a separate optical characterization board with a 1 mm^2 photodiode and transimpedance amplifier (TIA). We repeated the wireless power transfer measurements with the addition of the optical test board suspended above the implant to measure the light intensity. Using the normalized spectral emission data of the LED, and the spectral responsivity data of the photodiode, we were able to establish a mathematical relationship between the measured photodiode current and the optical power (P_{PD}) incident on the photodiode. We performed measurements of the photodiode current for different P_{LED} and far-field distances (3.01 mm to 8.01 mm). In practice, the optical stimulator would be positioned very close to the target (likely within ~100's μm), but we are limited to a 3.01 mm minimum distance because of the bulky, hermetically sealed packaging surrounding the available photodiode. We derived predicted optical power by performing a weighted integration of the LED radiation pattern over the solid angle occupied by the photodiode. The measurements agreed well with calculation, thus verifying our LED model. We found the LED to have ~10% electrical to optical efficiency (η_{LED}) over the entire power range of interest. Because the

refractive indices of mineral oil (n = ~1.4) and soft tissue (n = ~1.3-1.5) are very similar, Fresnel reflections at the LED interface would not differ significantly in practice. Optical losses in tissue can be kept small for short separation distances between the optical source and illumination target. We estimate the average optical intensity at the face of the LED, assuming a uniform surface emitter, for a given P_{LED} as $I_{opt} = (\eta_{LED} \times P_{LED})/A_{LED}$. This calculation ignores the diffraction that occurs in the LED packaging, which should be small. The active area (A_{LED}) of the LED is close to the size of typical fibers used in optogenetic stimulation, so the illuminated area is comparable.

V. Optogenetic Capabilities and Conclusions

Finally, we quantify the I_{acou} required to achieve optogenetic-level I_{opt} and stimulation patterns. Typical optogenetic PNS experiments use optical intensities of 1-15 mW/mm^2, though most stimulation artifacts can be achieved with the lower intensities [2], [3]. Most applications use light bursts instead of continuous illumination with duty cycles (D) up to 10% [2], [3]. The FDA regulated, time-averaged acoustic intensity is 7.2 mW/mm^2 for diagnostic imaging [8]; therefore, the peak acoustic intensity can be increased inversely with D, achieving higher optical intensities, while still meeting the FDA regulation. We also remain far below the FDA allowed spatial peak acoustic intensity of 1.9 W/mm^2 [8]. Using (2), along with our measurements, we establish I_{opt} as a function of the average I_{acou} - as shown in Fig. 3 for different D. Under continuous illumination, we can provide ~7 mW/mm^2 of light. With more practical duty cycles (< 10%), we can achieve very high optical intensities with just fractions of the FDA limit. For example, with a relatively large 10% duty cycle, we achieve 15 mW/mm^2 of optical intensity with just 26% of the FDA limit. Since the transmitted patterns are controlled externally with a sophisticated source, we can achieve any practical pulse-width or frequency of stimulation.

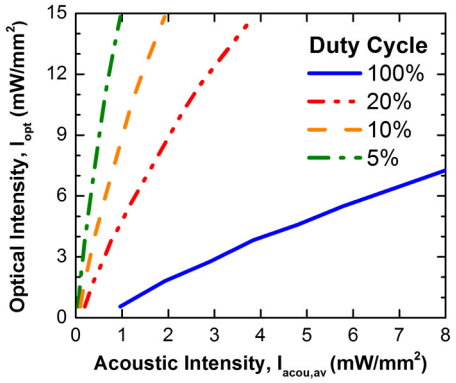

Fig. 3. The achieved optical intensity as a function of the average acoustic intensity, for different duty cycles.

Finally, we performed a fully wireless demonstration generating a practical optogenetic stimulation pattern by modulating the external source and measuring the resulting light pulses. Fig. 4 shows the measured output voltage of the TIA corresponding to a stimulation pattern with a repetition rate of 50 Hz, a pulse width of 2 ms (duty cycle of 10%), and an optical intensity of 15 mW/mm^2. This analysis shows that our system can achieve nearly any practical stimulation pattern for optogenetics, with safe wireless power delivery and externally programmable control.

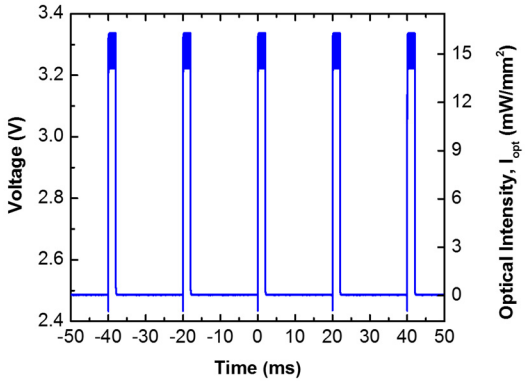

Fig. 4. Output voltage of the TIA and optical intensity of modulated light pulses with 50 Hz frequency and 2 ms pulse-width. Dark blue areas are 955 kHz ripple from capacitive feedthrough - this has no impact on the optical measurements.

Acknowledgement

This material is based upon work supported by the National Science Foundation Graduate Research Fellowship Program under Grant No. DGE-114747, the Yansouni Family Stanford Graduate Fellowship (SGF), and the DARPA Young Faculty Award (YFA).

References

[1] K. Famm *et al.*, "Drug discovery: A jump-start for electroceuticals," *Nature*, vol. 496, pp. 159-161, Apr. 2013.

[2] H. Liske, X. Qian, P. Anikeeva, K. Deisseroth, and S. Delp, "Optical control of neuronal excitation and inhibition using a single opsin protein, ChR2," *Sci. Rep.*, vol. 3, Oct. 2013.

[3] H. Liske *et al.*, "Optical inhibition of motor nerve and muscle activity *in vivo*," *Muscle Nerve*, vol. 47, Apr. 2013.

[4] J. Charthad, M. J. Weber, T. C. Chang, M. Saadat, and A. Arbabian, "A mm-sized implantable device with ultrasonic energy transfer and RF data uplink for high-power applications," *IEEE CICC,* Sep. 2014.

[5] J. Charthad, M. J. Weber, T. C. Chang, and A. Arbabian, "A mm-sized implantable medical device (IMD) with ultrasonic power transfer and a hybrid bi-directional data link," *IEEE Journal of Solid-State Circuits*, vol. 50, no. 8, Aug. 2015.

[6] H. Azhari. *Basics of Biomedical Ultrasound for Engineers*. Hoboken, NJ, Wiley, 2010, pp. 313-314.

[7] F. Mazzilli *et al.*, "Ultrasound energy harvesting system for deep implanted-medical-devices (IMDs)," in *Proc. IEEE Int. Symp. Circuits Syst.*, 2012.

[8] "Information for Manufacturers Seeking Marketing Clearance of Diagnostic Ultrasound Systems and Transducers," Food and Drug Administration, Rockville, MD, 2008.